

Degenerate two-photon Rydberg atom voltage reference ^{EP}

Cite as: AVS Quantum Sci. 4, 024403 (2022); <https://doi.org/10.1116/5.0090892>

Submitted: 09 March 2022 • Accepted: 26 May 2022 • Published Online: 15 June 2022

 C. Teale, J. Sherman and  J. Kitching

COLLECTIONS

Paper published as part of the special topic on [Quantum Sensing as a Technology](#)

 This paper was selected as an Editor's Pick



View Online



Export Citation

ARTICLES YOU MAY BE INTERESTED IN

[Optical measurements on a budget: A 3D-printed ellipsometer](#)

American Journal of Physics **90**, 445 (2022); <https://doi.org/10.1119/10.0009665>

[Call for papers on environment, sustainability, and climate change](#)

The Physics Teacher **60**, 323 (2022); <https://doi.org/10.1119/10.0010392>

[Chinese Abstracts](#)

Chinese Journal of Chemical Physics **35**, i (2022); <https://doi.org/10.1063/1674-0068/35/02/cabs>



Advance your science and career as a member of



AVS

LEARN MORE 

Degenerate two-photon Rydberg atom voltage reference

Cite as: AVS Quantum Sci. **4**, 024403 (2022); doi: [10.1116/5.0090892](https://doi.org/10.1116/5.0090892)

Submitted: 9 March 2022 · Accepted: 26 May 2022 ·

Published Online: 15 June 2022



View Online



Export Citation



CrossMark

C. Teale,^{a)}  J. Sherman, and J. Kitching 

AFFILIATIONS

Time and Frequency Division, National Institute of Standards and Technology (NIST), Boulder, Colorado 80305, USA

Note: This paper is part of the special topic collection, Quantum Sensing as a Technology.

^{a)}Electronic mail: carson.teale@nist.gov

ABSTRACT

We implement a DC voltage reference by measuring Stark shifts of cesium Rydberg atoms in a vapor cell. Cesium atoms are excited from the ground state to the 15s state via a degenerate two-photon transition that provides a narrow, Doppler free line. The 15s state experiences a scalar, quadratic Stark shift, which is used to measure the voltage across a parallel plate capacitor integrated into the vapor cell. We demonstrate a sensitivity of $82 \text{ mV}/\sqrt{\text{Hz}}$ at a bias voltage of 100 V. The device could be adapted for even larger voltages by increasing the plate spacing or using a lower energy state.

Published by AIP Publishing. <https://doi.org/10.1116/5.0090892>

Recently, Rydberg atoms have been used extensively in the measurement of RF electric field amplitudes by measuring the Autler–Townes splitting of a resonant RF transition.¹ This technique relates the electric field amplitude to a frequency measurement of the splitting through fundamental constants. The sensitivity of these RF E-field devices relies on the large transition dipole moments between nearby Rydberg states, which scales as n^2 , where n is the principal quantum number. For off-resonant RF fields, the energy shift due to the ac Stark effect can be measured.² In that case, the frequency shift is proportional to the square of the electric field and the polarizability of the state, α , which scales as n^7 .

The same measurement can be performed for a DC field, where the Stark shift is again proportional to the square of the electric field (for non-degenerate energy levels) and the polarizability. This has been done using the same electromagnetically induced transparency (EIT) excitation and detection technique as for RF measurements^{3–9} with sensitivities down to 10 mV/cm. DC electric field measurements have also been performed through direct UV excitation and pulsed field ionization detection with 20 $\mu\text{V}/\text{cm}$ sensitivity¹⁰ and using entangled Schrodinger-cat states¹¹ with a sensitivity of 30 ($\mu\text{V}/\text{cm}$)/ $\sqrt{\text{Hz}}$. A voltage measurement can be performed in a similar manner by solving Laplace’s equation to obtain the relation between the electric field at the point of measurement and the voltage applied to the electrodes. For an infinite, parallel plate capacitor, this takes the simple form $E = V/d$, where E is the electric field, V is the voltage, and d is the plate spacing. This is an accurate approximation for a finite, parallel plate capacitor so

long as the ratio of the length of the plates to the spacing is sufficiently large. If the plate spacing can be accurately measured, for example by using interferometric techniques, an accurate voltage measurement can be made.¹² Often a voltage reference is needed where stability is more critical than accuracy. In that case, the plate spacing would only need to be held constant while the voltage across the plates is controlled to keep the Stark shift locked to a particular frequency.

Compact optical frequency references using two-photon transitions in atomic vapor cells have been demonstrated^{13,14} with instabilities down to $4 \times 10^{-13}/\sqrt{\tau}$. Using similar techniques to lock a laser to a Rydberg energy level Stark shifted by 1 GHz (60 V/mm for the 15s state in Cs or 4 V/mm for the 30s state) would result in a fractional uncertainty in the E-field measurement of 10^{-7} after one second of averaging (assuming a similar optical frequency instability could be achieved). This is comparable to the short-term stabilities in the best zener diode voltage references.¹⁵ However, this sort of atomic voltage reference could operate at a wide range of different output voltages without the need for resistive or capacitive voltage dividers. In addition, future atomic devices could have better intrinsic accuracy than the best zener diodes, which have tolerances¹⁶ of 0.05%. Polarizability values have been measured¹⁷ to a part in 10^5 and the plate spacing could be determined interferometrically to a part in 10^6 for a 1 mm plate spacing.

In this work, we apply Rydberg atom electrometry to produce a sensitive and stable voltage reference. To do so, we measure Stark shifts of cesium Rydberg atoms inside a vapor cell with internal,

parallel plate electrodes. The quadratic Stark shift (applicable for non-degenerate states) is given by

$$f_s = \frac{\alpha}{2} E^2 = \frac{\alpha}{2} \left(\frac{V}{d} \right)^2. \quad (1)$$

The choice of which Rydberg state to use is a compromise between sensitivity, which improves with increasing polarizability, and voltage range. Higher-lying Rydberg states have level crossings that occur at lower voltages, resulting in a reduced range of quadratic behavior. We chose to use the 15s state which has its first level crossing around 1500 V/cm and a polarizability of 0.5 Hz/(V/m). With our electrode spacing of 5 mm, this gives a voltage range of 750 V. The 6s to 15s two-photon transition has a narrow natural linewidth of 730 kHz.¹⁸ Selection rules dictate¹⁹ that $\Delta F = 0$ and $\Delta m_F = 0$, which results in little sensitivity to magnetic fields since ground and excited states shift together. Higher angular momentum states, with linear Stark shifts and larger energy shifts with electric field, could potentially be populated using a similar excitation scheme if a large electric field provided enough state mixing to allow a two-photon transition directly to a high l state from the ground state s level. This idea was not experimentally investigated here.

The energy level diagram with all relevant states is shown in Fig. 1(a). The two-photon transition from the 6s state to the 15s state has a wavelength of 656 nm. The $6p_{3/2}$ level is the nearest intermediate state with a large detuning of about 100 THz, resulting in a low absorption cross-section. This low absorption cross-section leads to a small excitation rate and negligible excited state population fraction. Minimal Rydberg ionization rates are expected due to this small excited state population and relatively low energy of the 15s state. The atoms radiatively decay out of the 15s state via multiple channels, producing light spread across a range of wavelengths. In the current

experiment, all fluorescence with wavelengths of 550 nm or less is collected and used to determine the population of the excited state.

Figure 1(b) shows a diagram of the experiment. An external cavity diode laser (ECDL) with 20 mW of power injection locks a higher power (50 mW) laser diode which is amplified to 180 mW by a tapered amplifier. The linearly polarized optical field propagates through a reference cell with no electrodes and then through a cell with internal electrodes before being reflected back along the same path. This counter-propagating geometry is intrinsically Doppler-free and atoms in all velocity classes contribute to the fluorescence signal.²⁰ The beam is focused down to a waist size of 35 μm in each cell. Each cell has a photomultiplier tube (PMT) with a collection lens and short pass filter at 550 nm in front to capture the fluorescence signal, with a collection efficiency of about 3%. The electrode cell is shown in Fig. 1(c). It has internal, stainless steel electrodes (15 \times 60 mm²) separated by 5 mm. Internal electrodes are used to avoid shielding effects due to conductive Cs layers deposited on the walls of the cell²¹ and to avoid additional uncertainty in the electric field that would be caused by the glass dielectric. The electrode cell was held at a temperature of 70 °C while the reference cell was held at 90 °C. The expected transit time broadening in the electrode cell at this temperature and beam waist size is 5.7 MHz.

Figure 2(a) shows the fluorescence signal versus the frequency of the laser for various electrode voltages. In these measurements, the laser was not locked and its drift was accounted for by simultaneously measuring the fluorescence signal from the reference cell. The peak from the reference cell was used to align the frequency axis for each scan at a different voltage. Stark shifts were measured by locking the pump laser to the fluorescence signal from the electrode cell using standard FM spectroscopy. The frequency of a beat note between the locked laser and an optical frequency comb (with a fractional

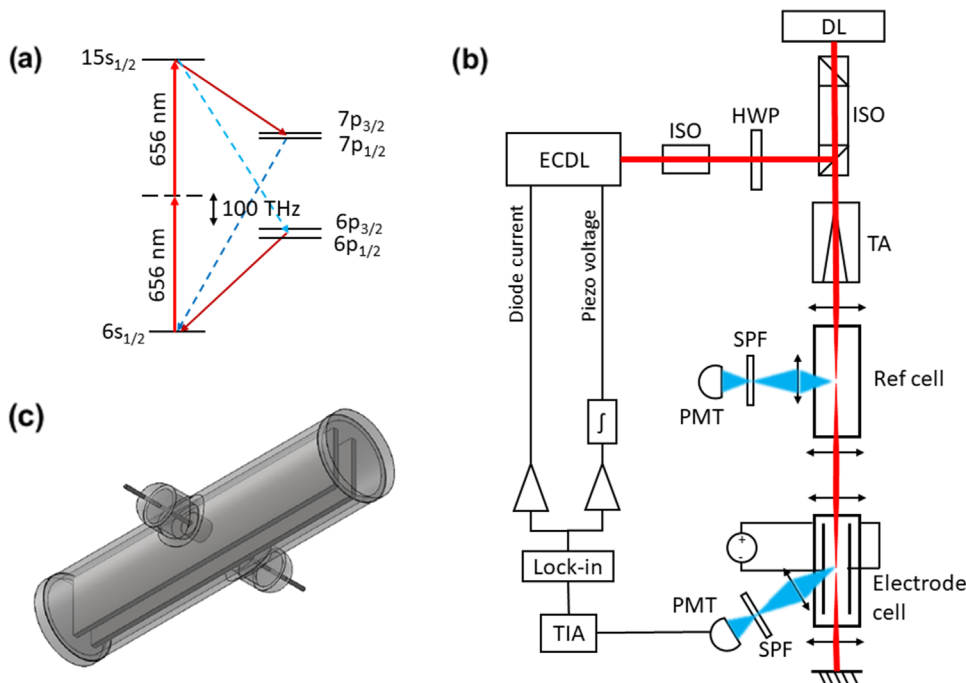


FIG. 1. (a) Energy level diagram of Cs and the degenerate two-photon transition to the 15s state at 656 nm, which is detuned by about 100 THz from the nearest intermediate level. (b) Schematic of experiment. ECDL: external cavity diode laser, ISO: isolator, HWP: half wave plate, DL: diode laser, TA: tapered amplifier, SPF: short pass filter, PMT: photomultiplier tube, TIA: trans-impedance amplifier. (c) Drawing of glass-blown Cs vapor electrode cell with internal, stainless steel electrodes.

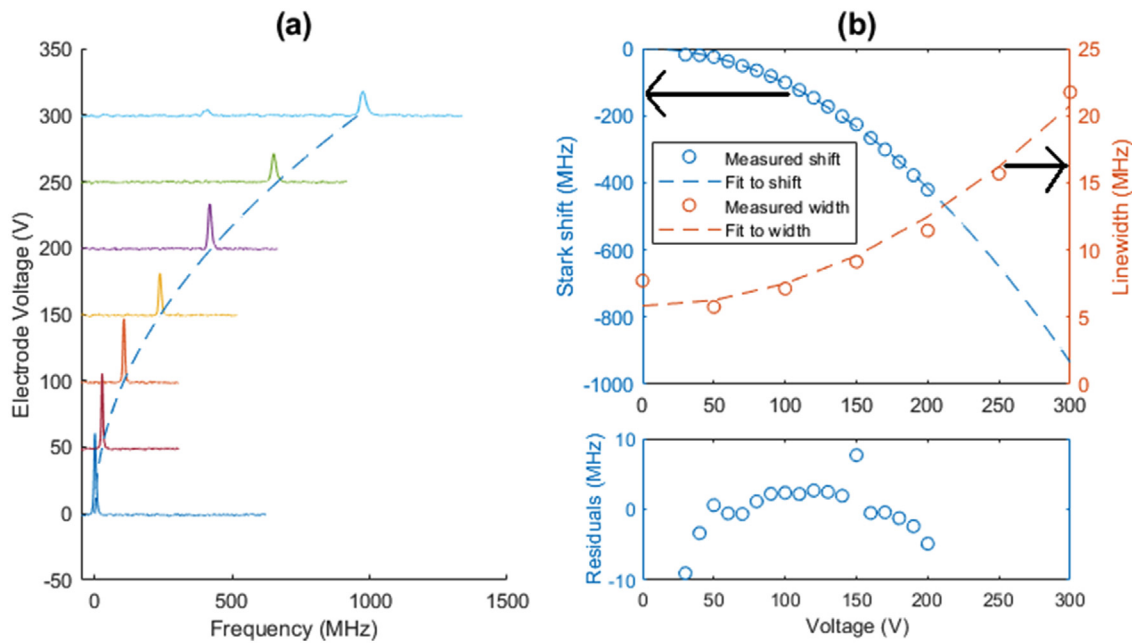


Fig. 2. (a) Fluorescence signal vs laser frequency at various electrode voltages (dashed line shows quadratic fit to peak centers). (b) Stark shift measured using beat note with frequency comb (left axis) and transition linewidths (right axis). The larger 8 MHz linewidth at 0 V bias appeared to be an anomaly of this particular dataset. Other measurements at 0 V resulted in linewidths closer to 5.7 MHz. The fit to the measured shifts takes the form $f_s = \alpha_1 V^2$ and the fit to the measured widths takes the form $\gamma = \alpha_2 V^2 + \beta$. Residuals of quadratic fit to measured Stark shifts are shown below.

frequency stability of better than 10^{-13} at one second) with a 250 MHz repetition rate was measured for various voltages applied across the internal electrodes. The two beams were overlapped on a fast photodiode and a low pass filter at 100 MHz isolated the beat note of interest which was then measured by a frequency counter. These results are shown in Fig. 2(b). A quadratic fit resulted in a polarizability measurement of $0.52 \text{ Hz}/(\text{V}/\text{m})^2$ with a statistical uncertainty of about 1%, which is in perfect agreement with the theoretically calculated value^{22,23} of $0.52 \text{ Hz}/(\text{V}/\text{m})^2$. However, because we have not carefully assessed the systematics in this measurement, we are unable at present to determine the accuracy of the experimentally determined polarizability value. The residuals of the quadratic fit are also shown in Fig. 2(b). These deviations from a quadratic are much larger than the deviations caused by the presence of the energy level crossing at 750 V (calculated by direct diagonalization of the Hamiltonian), and we do not understand the source of these deviations as of yet. We observe approximately a 1% deviation from quadratic scaling at 200 V, which represents a significant limit to the accuracy of the device. The linewidth at zero field is 5.7 MHz while field inhomogeneities result in the linewidth broadening (approximately quadratically with bias voltage) to 22 MHz at 300 V, as shown in Fig. 2(b). The linewidth goes quadratically with voltage since the broadening is due to atoms seeing different electric fields at different positions. Since the stark shift goes quadratically with the field, so too does the difference in stark shifts. The broadened, 22 MHz linewidth observed at 300 V bias could be explained by a 540 V/m difference in electric field across the spatial extent of the measurement area. The largest spatial dimension of the measurement region is given by the Rayleigh range of the beam (6 mm).

Assuming the gradient is along this dimension results in an estimated fractional field gradient of 1.5%/cm.

The voltage sensitivity (the minimum detectable change in voltage at a given integration time) is dependent on the linewidth of the transition, the signal to noise ratio and the voltage bias. The local slope of the Stark shift versus voltage grows steeper for increasing voltage bias, resulting in better sensitivity according to

$$\frac{\partial f_s}{\partial V} = \frac{\alpha V}{d^2}. \tag{2}$$

Figure 3(a) shows the fluorescence signal for both the Stark shifted electrode cell at 100 V bias and the reference cell. Figure 3(b) displays the sensitivity of the device out to 6 kHz. This was measured by applying a 40 Hz, 1 V peak-to-peak modulation to the electrodes in addition to the DC voltage. The 40 Hz RMS voltage at the output of the lock-in was measured and used to scale the noise power spectral density at the lock-in output into a sensitivity. The average sensitivity over the 6 kHz bandwidth was $82 \text{ mV}/\sqrt{\text{Hz}}$. On resonance, the fluorescence power from the electrode cell was 150 fW and the measured noise on this signal was $0.22 \text{ fW}/\sqrt{\text{Hz}}$, close to the calculated shot noise of $0.27 \text{ fW}/\sqrt{\text{Hz}}$. The shot noise from scattered laser light was comparable to the shot noise from the fluorescence and the noise floor from stray room light was ten times lower than the noise from fluorescence and laser scatter. The tone frequency applied to the electrodes was increased out to 1 kHz with measured sensitivities remaining constant. The ultimate limit of the bandwidth of the device is likely determined by the linewidth of the transition.

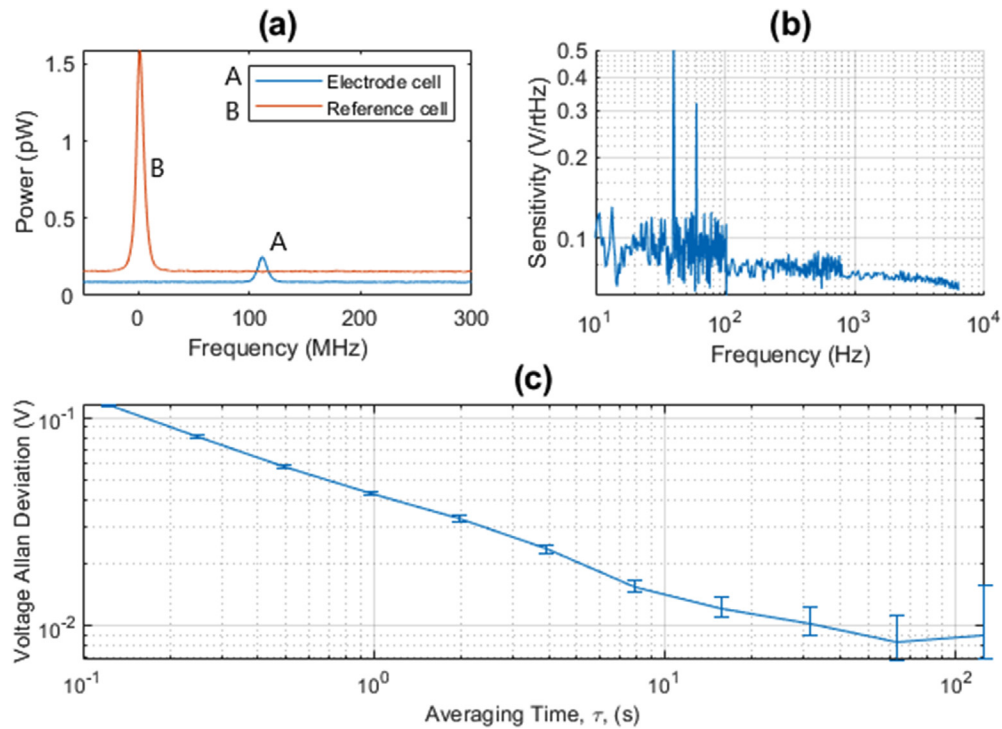


FIG. 3. (a) Fluorescence signal from electrode cell (A) and reference cell (B) at 100 V. 100 scans were averaged together for this plot. (b) Measured sensitivity of the voltage reference. The signal at 40 Hz is due to the 1 V_{p-p} voltage applied to the electrodes. (c) Voltage Allan deviation as a function of averaging time with 100 V bias (error bars represent 68% confidence intervals).

Figure 3(c) shows the voltage stability as a function of integration time. This was measured by again counting the frequency of the beat note between the optical frequency comb and the laser locked to the stark shifted resonance with a constant 100 V applied across the electrodes. The beat note frequencies were converted to voltage variations by dividing by the measured slope of the Stark curve [Fig. 2(b)]. As expected for a shot noise limited system, the sensitivity averages down at a rate of $1/\sqrt{\tau}$ for short integration times. Measurements were limited to 1000 s due to difficulty maintaining laser injection locking.

As it is now, the instrument performs the function of a voltmeter, but could be made into a true voltage reference by incorporating a tunable voltage source in a feedback loop. The beat note described above would be phase locked to another local oscillator by feeding back to the voltage across the electrodes. The Stark shift could also be measured using a single laser and acousto-optic modulator (AOM) instead of using an optical frequency comb. The laser would be split with the AOM, one beam locked to the reference cell and the other locked to the electrode cell. The AOM frequency would directly readout the Stark shift.

The $82 \text{ mV}/\sqrt{\text{Hz}}$ sensitivity could be improved by increasing the beam waist to reduce transit time broadening while also increasing the laser power. For example, the cell could be placed within a build-up cavity,²⁴ increasing the power by a factor of 20 or more and therefore the fluorescence signal strength by a factor of 400 or more (assuming the same beam waist). Field inhomogeneities could be reduced through more careful electrode construction to reduce broadening at

larger bias voltages. In the glass blown cell, we suspect that field inhomogeneities are primarily due to manufacturing defects because of visible irregularities in the electrode surfaces and measured, relative tilt between the two electrodes. Surface patch charges are thought to be a smaller effect since the atoms are largely shielded from the glass walls by the electrodes. We also expect less photoionization due to the lower energy 656 nm photons, than has been reported in other studies.⁸ We plan to fabricate microelectromechanical systems (MEMs) based vapor cells with integrated electrodes that could be made with more precise dimensional tolerances.¹² With these improvements, parts per million uncertainties could be achieved on 100 V after one second of averaging. Sources of drift include light shifts due to laser power fluctuations and changes in the electrode spacing due to temperature fluctuations of the cell. Achieving ppm voltage uncertainty at 100 V would require laser amplitude stabilization to better than 0.1% due to the large light shift (estimated at 90 kHz) at full intensity (180 mW across a 35 μm waist). The fractional uncertainty in the voltage is directly proportional to the fractional uncertainty in the plate spacing, which is determined by the thermal expansion coefficient and variations in cell temperature. To achieve ppm level voltage stabilities with glass as the material between the electrodes would require temperature stabilization of 0.25 °C if no active measurement of the plate separation were implemented. *In situ* interferometric measurements of the plate spacing with a known wavelength could improve the stability further and enable an accurate voltage determination to the extent that the atomic polarizability is known.

We predict that short-term stabilities of future Rydberg atom voltmeters could be comparable to the best commercial high voltage references based on solid state references. With more accurate determinations of polarizability values and by incorporating plate spacing measurements into the device, built-in accuracies of a part in 10^5 could also be achieved in future devices.

ACKNOWLEDGMENTS

The authors thank Chris Holloway, Nikunj Kumar Prajapati, Alain Rufenacht, Sam Benz, Paul Dresselhaus, and Matt Hummon for valuable discussions. Funding was provided by the National Institute of Standards and Technology.

AUTHOR DECLARATIONS

Conflict of Interest

The authors declare no conflict of interest.

DATA AVAILABILITY

The data that support the findings of this study are available from the corresponding author upon reasonable request.

REFERENCES

- ¹H. Fan, S. Kumar, J. Sedlacek, H. Kübler, S. Karimkashi, and J. P. Shaffer, *J. Phys. B* **48**, 202001 (2015).
- ²D. H. Meyer, Z. A. Castillo, K. C. Cox, and P. D. Kunz, *J. Phys. B* **53**, 034001 (2020).
- ³A. K. Mohapatra, M. G. Bason, B. Butscher, K. J. Weatherill, and C. S. Adams, *Nat. Phys.* **4**, 890 (2008).
- ⁴R. Daschner, R. Ritter, H. Kübler, N. Frühauf, E. Kurz, R. Löw, and T. Pfau, *Opt. Lett.* **37**, 2271 (2012).
- ⁵D. Barredo, H. Kübler, R. Daschner, R. Löw, and T. Pfau, *Phys. Rev. Lett.* **110**, 123002 (2013).
- ⁶M. G. Bason, M. Tanasittikosol, A. Sargsyan, A. Mohapatra, D. Sarkisyan, R. Potvliege, and C. Adams, *New J. Phys.* **12**, 065015 (2010).
- ⁷A. Tauschinsky, R. M. Thijssen, S. Whitlock, H. van Linden van den Heuvell, and R. Spreuw, *Phys. Rev. A* **81**, 063411 (2010).
- ⁸Y.-Y. Jau and T. Carter, *Phys. Rev. Appl.* **13**, 054034 (2020).
- ⁹R. P. Abel, C. Carr, U. Krohn, and C. S. Adams, *Phys. Rev. A* **84**, 023408 (2011).
- ¹⁰A. Osterwalder and F. Merkt, *Phys. Rev. Lett.* **82**, 1831 (1999).
- ¹¹A. Facon, E.-K. Dietsche, D. Grosso, S. Haroche, J.-M. Raimond, M. Brune, and S. Gleyzes, *Nature* **535**, 262 (2016).
- ¹²J. Kitching, E. A. Donley, S. Knappe, M. Hummon, A. T. Dellis, J. Sherman, K. Srinivasan, V. A. Aksyuk, Q. Li, D. Westly, B. Roxworthy, and A. Lal, *J. Phys.* **723**, 012056 (2016).
- ¹³K. W. Martin, G. Phelps, N. D. Lemke, M. S. Bigelow, B. Stuhl, M. Wojcik, M. Holt, I. Coddington, M. W. Bishop, and J. H. Burke, *Phys. Rev. Appl.* **9**, 014019 (2018).
- ¹⁴V. Maurice, Z. L. Newman, S. Dickerson, M. Rivers, J. Hsiao, P. Greene, M. Mescher, J. Kitching, M. T. Hummon, and C. Johnson, *Opt. Express* **28**, 24708 (2020).
- ¹⁵T. Witt, D. Reymann, and D. Avrons, *IEEE Trans. Instrum. Meas.* **44**, 226 (1995).
- ¹⁶See <https://www.americanmicrosemi.com/tutorial/zener-diode/> for “American Microsemiconductor, Zener Diode.”
- ¹⁷J. A. Sherman, N. D. Lemke, N. Hinkley, M. Pizzocaro, R. W. Fox, A. D. Ludlow, and C. W. Oates, *Phys. Rev. Lett.* **108**, 153002 (2012).
- ¹⁸C. E. Theodosiou, *Phys. Rev. A* **30**, 2881 (1984).
- ¹⁹K. D. Bonin and T. J. McIlrath, *J. Opt. Soc. Am. B* **1**, 52 (1984).
- ²⁰G. Grynberg and B. Cagnac, *Rep. Prog. Phys.* **40**, 791 (1977).
- ²¹M. A. Bouchiat, J. Guéna, P. Jacquier, M. Lintz, and A. V. Papoyan, *Appl. Phys. B* **68**, 1109 (1999).
- ²²W. van Wijngaarden and J. Li, *J. Quant. Spectrosc. Radiat. Transfer* **52**, 555 (1994).
- ²³N. Šibalić, J. Pritchard, C. Adams, and K. Weatherill, *Comput. Phys. Commun.* **220**, 319 (2017).
- ²⁴T. Uehara, K. Sugiyama, and M. Kitano, “Frequency stabilization of laser diode to the 6s-8s two-photon transitions in cesium atoms in a vapor cell placed in an external cavity,” in *2012 Conference on Precision Electromagnetic Measurements* (IEEE, 2012), pp. 268–269.